Structure of a Magnetic Flux Annihilation Layer Formed by the Collision of Supersonic, Magnetized Plasma Flows

L. G. Suttle, J. D. Hare, S. V. Lebedev, G. F. Swadling, G. C. Burdiak, A. Ciardi, J. P. Chittenden, N. F. Loureiro, N. Niasse, F. Suzuki-Vidal, J. Wu, Q. Yang, T. Clayson, A. Frank, T. S. Robinson, R. A. Smith, and N. Stuart

Phys. Rev. Lett. **116**, 225001 — Published 31 May 2016

DOI: 10.1103/PhysRevLett.116.225001

Structure of a magnetic flux annihilation layer formed by the collision of supersonic, magnetized plasma flows

L. G. Suttle,[1] J. D. Hare,[1] S. V. Lebedev,[1] G. F. Swadling,[1†] G. C. Burdiak,[1] A. Ciardi[2,3], J. P. Chittenden,[1] N. F. Loureiro[4], N. Niasse,[1] F. Suzuki-Vidal,[1] J. Wu,[5] Q. Yang,[6] T. Clayson,[1] A. Frank,[7] T. S. Robinson,[1] R. A. Smith,[1] N. Stuart[1]

[1]*Blackett Laboratory, Imperial College, London, SW7 2BW, United Kingdom*
[2]*Sorbonne Universités, UPMC Univ. Paris 6, UMR 8112, LERMA, F-75005, Paris, France*
[3]*LERMA, Observatoire de Paris, PSL Research University, CNRS, UMR 8112, F-75014, Paris France*
[4] *Plasma Science and Fusion Center, Massachusetts Institute of Technology, Cambridge MA 02139, USA*
[5]*State Key Laboratory of Electrical Insulation and Power Equipment, Xi'an Jiaotong University, Xi'an 710049, China*
[6] *Institute of Fluid Physics, China Academy of Engineering Physics, Mianyang 621900, China*
[7]*Department of Physics and Astronomy, University of Rochester, Rochester, New York 14627, USA*
e-mail address: l.suttle10@imperial.ac.uk, s.lebedev@imperial.ac.uk
[†]*Current address: Lawrence Livermore National Laboratory, California 94550, USA*

We present experiments characterizing the detailed structure of a current layer, generated by the collision of two counter-streaming, supersonic and magnetized aluminum plasma flows. The anti-parallel magnetic fields advected by the flows are found to be mutually annihilated inside the layer, giving rise to a bifurcated current structure – two narrow current sheets running along the outside surfaces of the layer. Measurements with Thomson scattering show a fast outflow of plasma along the layer and a high ion temperature ($T_i \sim \bar{Z}T_e$, with average ionization $\bar{Z}=7$). Analysis of the spatially resolved plasma parameters indicates that the advection and subsequent annihilation of the inflowing magnetic flux determines the structure of the layer, while the ion heating could be due to the development of kinetic, current-driven instabilities.

DOI: **PACS:**

The interaction of supersonic, counter-streaming plasma flows occurs in many astrophysical scenarios (e.g. astrophysical jets [1], termination shocks [2,3]) and in laboratory experiments (e.g. colliding plasmas in ICF hohlraums [4]). The presence of frozen-in magnetic fields advected by the colliding flows could play an important role in determining the structure of the interaction region in these systems. Collisions of magnetized plasmas with oppositely directed magnetic fields should eventually lead to annihilation of the flux via magnetic reconnection. In many astrophysical scenarios reconnection occurs in high beta plasmas and is strongly driven, with ram pressure significantly exceeding the magnetic pressure. The structure of the reconnection layer in these conditions is unknown, but is expected to adjust to accommodate the rate of magnetic flux delivered into the layer, where for example, a pile-up of the magnetic flux could contribute to controlling the reconnection rate [5,6]. A number of recent laser-driven, high energy density physics (HEDP) experiments [7–10] have investigated magnetic reconnection in the strongly driven regime, as well as the formation of astrophysically relevant collisionless shocks [11] and self-organized field structures [12]. Large-scale field structures produced by collisions between laser-driven plasma flows have for example been interpreted [11] as being due to the accumulation of advected toroidal magnetic fields generated via the Biermann battery mechanism at the laser spots [13]). Despite the importance of magnetic fields in defining the properties of shocks formed in HEDP plasmas, experimental information is however still limited.

In this letter we present experimental data characterizing the structure of an interaction layer formed by the collision of two counter-streaming, supersonic (sonic Mach number $M_S>3$), magnetized plasma flows. These flows advect embedded magnetic fields (Magnetic Reynolds number $Re_M>30$), orientated in opposing directions perpendicular to the flow, and their interaction is strongly driven [i.e. high dynamic Beta regime, $\beta_{dyn}=\rho V_{flow}^2/(B^2/2\mu_0)\sim 7$]. The experiments provide detailed, simultaneous, spatially-resolved measurements of the key plasma parameters: flow velocities and temperatures via Thomson scattering, the distribution of the magnetic field via polarimetry, and the electron density distribution via laser interferometry. We observe the formation of a thin current layer (half-thickness $\delta\approx 0.5$mm, comparable to the ion inertial length c/ω_{pi}), which is supported by the balance between the ram pressure of the flow and the thermal pressure inside the layer, for a time significantly exceeding the expected characteristic hydrodynamic timescale ($\tau_{layer}>20\delta/V_{flow}$). The measured magnetic field distribution indicates that the destruction of magnetic flux takes place at the layer surfaces, consistent with two narrow, localized current sheets. Measurements

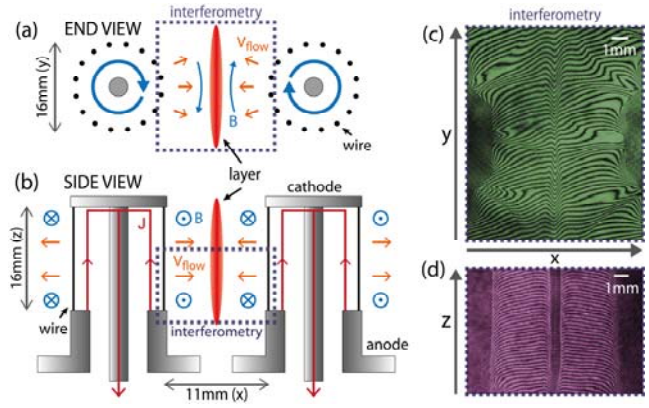

FIG.1 Cross-sectional schematic diagrams of the production of two magnetized, colliding plasma flows from (a) end and (b) side views. (c,d) Corresponding interferograms of the structure of the interaction region from each perspective (fields of view indicated in schematics).

also show a high ion temperature in the layer ($T_i \sim \bar{Z}T_e$, with $\bar{Z}$~7).

The experiments were carried out at the MAGPIE pulsed power facility [14] using the set-up illustrated in Fig. 1a & b. The supersonic counter-streaming plasma flows are produced by the ablation of thin aluminum (Al) wires driven by a 1.4MA, 250ns-rise current pulse. These are arranged to form two cylindrical "exploding" wire arrays [15], with the total current equally divided between the two arrays. The current J in each array runs up the wires and returns through the central conductor, as indicated in Fig. 1a. Ablation flows form in a similar manner to those produced by standard ("imploding") wire arrays [16–18], however here the J×B force acts to direct the plasma radially outwards, into a region initially free of magnetic fields. The ablated plasma is accelerated away from the wires, reaching a velocity of ~50km/s within the first 1-2mm, and thereafter propagates with an almost constant velocity. Previous measurements [19,20] have demonstrated that the plasma flows generated by a single exploding wire array have a frozen-in, azimuthal, advected magnetic field (B~2T), and are super-fast-magnetosonic. The arrays used in the current experiments consist of 16, 40μm-diameter Al wires, 16mm in length, positioned on a 16mm diameter (Fig. 1a). The gap between the two arrays is 11mm and they are driven in the same polarity, such that when the advected magnetic fields meet they are oriented in opposite directions, and their interaction should lead to the annihilation of the magnetic flux.

The interaction of the colliding plasmas was diagnosed using a range of diagnostics, allowing simultaneous measurements of the relevant plasma parameters with high spatial and temporal resolution. A Thomson scattering (TS) diagnostic [20,21] was used to record the ion feature of the collective TS spectrum, measuring the flow velocity and temperatures (T_i, $\bar{Z}T_e$) of the plasma. The distribution of magnetic field was measured using a polarimetry (Faraday rotation) diagnostic (1053nm, 1ns) [20], while the electron density was obtained in end-on (x-y) and side-on (x-z) directions via laser interferometry (532 and 355nm, 0.3ns, and 1053nm, 1ns) [20,22].

Typical end-on and side-on interferograms obtained at t=215ns after current start, when the interaction layer is fully formed are shown in Fig. 1c & d. In this letter we shall concentrate on the detailed characterization of the layer properties at this time. Measurements were performed at various times between t=160ns, when the layer becomes detectable by interferometry (electron line density $\int n_e dl$ corresponding to a ½-fringe shift), and t=265ns, when the drive current has passed its peak. These measurements indicated that while the density of the accumulated plasma increases with time, the overall structure of the layer and its thickness (2δ~1mm) remain constant. The interferograms are processed into maps of $\int n_e dl$ by applying the analysis procedure described in [20,22]. For the end-on data the maps can be further converted to electron density n_e, by dividing $\int n_e dl$ by the probing path length (i.e. array height), on the basis that the density structure is approximately uniform in the axial (z) direction.

The end-on electron density map (Fig. 2a, raw image in Fig. 1c) shows the radially diverging plasma flows produced by the wire arrays for the region indicated in Fig. 1a. The ablated plasma density close to each array is modulated azimuthally due to the use of a relatively small number of wires in these experiments (16 per array). The observed flow structure however evolves downstream of the wires via the oblique collision of the individual streams (as described in [19,22]), smoothing out these modulations in the region just upstream of the interaction layer. Comparison of radial profiles of the density at analogous azimuthal positions (e.g. profiles marked "1" and "2") shows that the upstream flow structure is not affected by the subsequent interaction, as should be expected for a supersonic flow. The collision of the opposing flows leads to the formation of a dense, axially-smooth, narrow layer in the mid-plane, extending across the length of the image in the y-direction, perpendicular to the flow. Within the layer, it is noted that the maximum density is not located at the

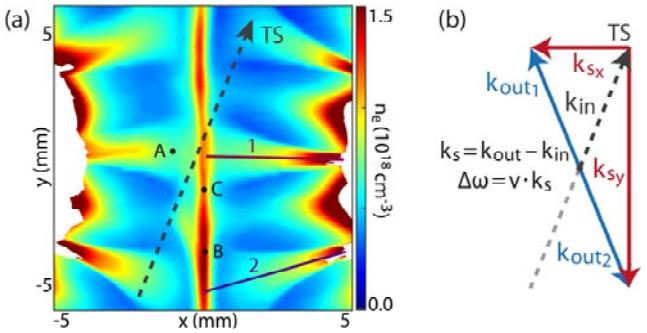

FIG.2 (a) End-on electron density map, obtained by interferometry, showing probing geometry of the Thomson scattering (TS) laser beam, and positions (black dots, A-C) of TS measurements whose spectra are shown in Fig. 3. (b) TS geometry vector diagram.

central position (x,y=0), despite it receiving the highest influx of material from the flows. This is due to a

symmetric outward plasma motion along the layer, which we directly measure using Thomson scattering.

The multi-point TS diagnostic, whose geometry is illustrated in Fig. 2, operated simultaneously with the interferometry measurements. The focused probing laser beam (532nm, 5ns FWHM, 3J, $\emptyset < 200\mu m$) propagated in the x-y plane, at an angle of 22.5° to the interaction layer. The position (y-coordinate) at which the probing beam crossed the layer was adjusted between different experiments to sample different regions of the plasma. The scattered light was collected in the same plane, from 13 spatial positions along the beam, at scattering angles of θ=45° & 135° to the laser, using an imaging spectrometer and two linear arrays of optical fibres (see [20,21] for more details). Alignment of the TS diagnostic and determination of the scattering volume locations with respect to the interferogram was performed as described in [20], with a precision of ≤0.2mm. The scattering geometry (Fig. 2b) produces separate measurements sensitive to the components of the flow velocity perpendicular (V_x) and parallel (V_y) to the interaction layer respectively. These are determined from the Doppler shift of the TS spectra as $\delta\omega_{D1}=k_{Sx}\cdot V_x$ and $\delta\omega_{D2}=k_{Sy}\cdot V_y$.

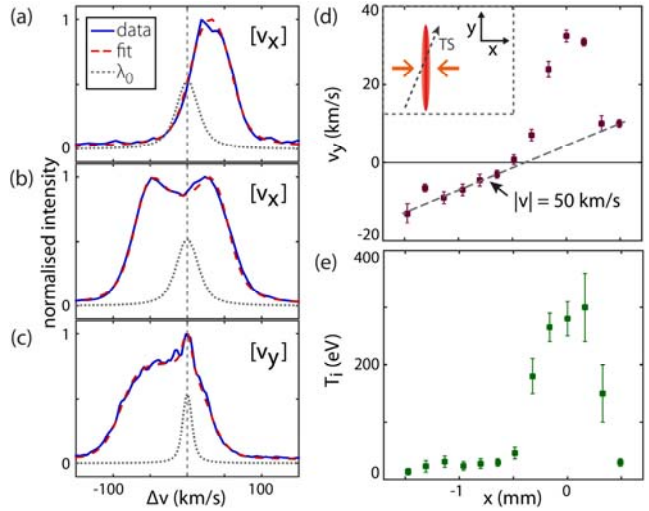

FIG.3 (a-c) Fitted TS spectra for the 3 spatial points in the interaction region marked in Fig. 2a. Dotted line (λ_0) indicates spectrometer resolution. (d,e) Profiles of $V_y(x)$ and $T_i(x)$ measured in a single experiment for scattering volumes along the TS beam when passing through position C in Fig. 2a.

Characteristic TS spectra from three key spatial positions in the interaction are shown in Fig. 3a-c. These spectra were recorded simultaneously with the interferometry data presented in Fig. 2a and their positions are marked in that figure (A-C, with black dots representing the spatial resolution of the measurements). The TS Data obtained upstream of the layer (e.g. position A, spectrum Fig. 3a) indicates that the flows approach the interaction layer with an incident velocity of approximately 50km/s in the direction normal to the layer. On crossing the layer boundary, this V_x component falls to zero (e.g. as shown in Fig. 3b), however we see that the plasma inside the interaction layer acquires significant motion in the perpendicular y-direction (e.g. Fig. 3c). Measurements at positions C (y=-1.0mm) and B (y=-3.7mm) yield V_y=-30km/s and -60km/s respectively, indicating an outward acceleration of material along the layer. Fig. 3d illustrates this motion in comparison to the plasma outside of the layer; V_y is plotted as a function of x for the 13 scattering positions along the probing TS beam in a single experiment (with the beam passing through position C in Fig. 2a). This shows that there is a clear perturbation within the layer from the linear velocity profile (dashed line) of the upstream plasma – this non-zero upstream V_y profile being due to the cylindrical divergence of the setup (Fig. 1a).

Fitting theoretical form factors to the measured TS spectra (similar to [20,23]) allows us to obtain plasma temperatures (Fig. 3e). We note that local temperatures obtained from fits to the spectra from each of the separate scattering directions (Fig. 2b) were in agreement. This strongly suggests that the shape of the scattering spectra is determined by thermal motion, and not by possible variations of the flow velocities inside the scattering volumes. The upstream plasma was found to be cold (T_i=22±10eV, T_e<20eV), while inside the layer the ion temperature rises rapidly, reaching T_i≈300eV at the most centrally measured position (C). The electron temperature in the layer is best determined from the spectra obtained for the 45° scattering angle (e.g. Fig. 3b), yielding $\bar{Z}T_e$=320±20eV. Using this measured value to constrain the magnitude of the product, a non-LTE model [24,25] can then be applied to calculate self-consistent values of $\bar{Z}$ and T_e, which provides a best estimate of average ionization $\bar{Z}$=7.3 and T_e=43eV. We emphasize that in all experiments the measured ion temperature significantly exceeded the electron temperature inside the layer, with $T_i \sim \bar{Z}T_e$.

The distribution of the magnetic field was measured using simultaneous side-on polarimetry and interferometry.

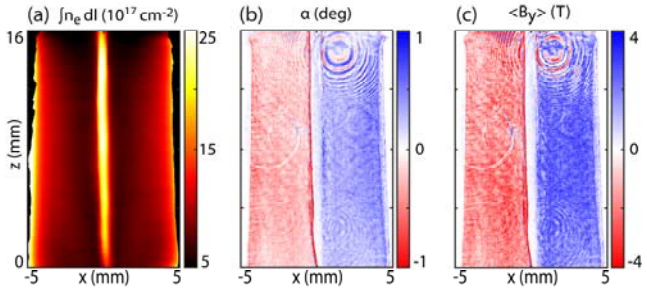

FIG.4 Side-on maps of the interaction region showing (a) electron line density (interferometry), (b) Faraday rotation angle, and (c) magnetic field. Ring structures evident in the data are artifacts caused by dust spots.

Polarimetry images were taken using two channels with oppositely rotated linear polarizers at ±3° from extinction. The Faraday rotation images were analyzed using the procedure described in detail in [20], yielding a 2-D map of the rotation angle $\alpha(x,z)$ as shown in Fig. 4b. It is seen that the rotation angle has different signs on the two sides of the

layer, as expected for the magnetic field geometry of this set-up (Fig. 1b). The Faraday rotation angle is determined by both the magnetic field and electron density [26]. The average magnetic field in the y-direction can be found by dividing the rotation angle by the line density:

$$B_y(x,z) = \frac{8\pi^2\varepsilon_0 m_e{}^2 c^3}{e^3\lambda^2}\frac{\alpha(x,z)}{\int(n_e(x,y,z)\cdot dy)} \quad (1)$$

and the resulting map is shown in Fig. 4c. The distribution of the magnetic field is approximately uniform in the z-direction, with some noise on smaller spatial scales due to the small values of the Faraday rotation angle (~1°). To reduce the effect of the noise we average in the z-direction over an interval of Δz=6mm in the middle of the image to produce the magnetic field profile of Fig. 5a. Outside the interaction layer B=±2T; the field then peaks in a narrow interval at the layer's surface before rapidly dropping to almost zero inside. The corresponding current density distribution ($j_z=-1/\mu_0\cdot\partial B_y/\partial x$) consists of two narrow, bi-directional current sheets located at the boundaries of the layer (Fig. 5b). This field structure is consistent with the compression of the advected magnetic field at the shock, followed by a rapid dissipation of the magnetic flux in a narrow (≈0.1mm) region at the boundary of the layer. The mean free paths for electrons and ions in the plasma are much shorter than the spatial scales involved ($\lambda_{ii}\sim\lambda_{ei}\sim3\mu$m), suggesting the plasma is strongly collisional. The magnetic field pile-up occurs at ⍰x⍰~0.5mm, which is comparable to the ion skin depth c/ω_{pi}~0.3-0.4mm. This suggests that two-fluid physics such as the Hall Effect play an important role in this system, as the ions decouple from the electrons on the scale at which we see flux pile-up.

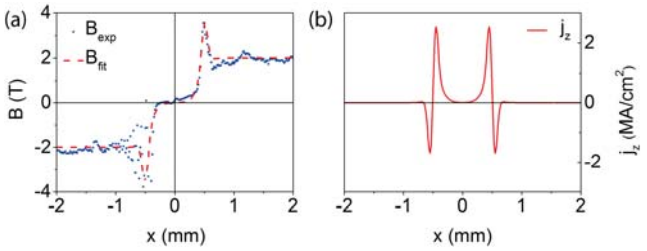

FIG.5 (a) z-averaged profile of the measured (blue dots) magnetic field $B_y(x)$, and (b) profile of the current density calculated for a fitted magnetic field profile shown by the red dashed line in (a).

The plasma layer formed in these experiments appears to be in dynamic equilibrium, maintaining an approximately constant thickness over a timescale much longer than the characteristic hydrodynamic time. Using the measured plasma parameters we find that there is a close balance between the ram pressure of the incoming flow and the thermal pressure of the plasma in the layer, and also between the ram pressure and the magnetic pressure of the piled-up field. We note that the magnetic pressure is not important in the upstream flow [$\rho V^2/(B^2/2\mu_0)=2M_A{}^2\sim7$], nor inside the layer, where the magnetic pressure is negligible in comparison to thermal pressure.

The energy balance presents a more complicated and interesting situation due to an unexpectedly high ion temperature ($T_i\approx300$eV) inside the layer. The 50km/s velocity measured upstream of the layer boundary, where T_i is small, corresponds to Al ions with a directed kinetic energy of E_i=340eV. Thermalization of this kinetic energy (assuming no energy is transferred to the electrons) gives a maximum possible ion temperature of $T_i=(2/3)E_i$=230eV. This is already smaller than the measured post-interaction T_i. The time for energy exchange between the electron and ion populations, $\tau_{ei}{}^E\sim$20ns, is much shorter than the life-time of the layer and should lead to $T_i\sim T_e$ and not $T_i\sim\bar{Z}T_e$. The expected post-shock plasma temperature corresponding to equilibration between the ion and electron temperatures can be estimated using a standard expression for heating in a strong shock [27]:

$$k_BT = E_i\frac{4(\gamma-1)}{(\gamma+1)^2}\frac{1}{(\bar{Z}+1)}. \quad (2)$$

Using γ=5/3 yields a much lower temperature of $T_i=T_e\sim30\rightarrow15$eV for $\bar{Z}=3\rightarrow7$, while the immediate post-shock ion temperature is $T_i\sim$120eV, corresponding to $\bar{Z}$=0 in the above formula.

These estimates suggest that the post-shock ion temperature should be significantly smaller than measured, even without taking into account energy losses to ionization and radiative cooling. This in turn suggests that there must be a mechanism providing continuous heating of the ions, in order to sustain both their high temperature and the large difference between the ion and electron temperatures.

The most plausible explanation for the observed ion heating is that it occurs in the current sheets formed at the boundaries of the layer. The large spatial gradients of the magnetic field seen in this region (Fig. 5) correspond to current densities of the order of ~1-2MA/cm^2, however resistive heating of the plasma by this current should only heat the electrons, and the subsequent transfer of energy to the ions cannot explain the observed $T_i\sim\bar{Z}T_e>>T_e$. Enhanced heating of the ions has been extensively discussed, e.g. in the context of magnetic reconnection studies [28–31], and is often associated with the development of current-driven kinetic plasma turbulence. The high current density at the boundary of the current layer corresponds to a velocity of the current-carrying electrons ($u_{ez}=j_z/en_e$) exceeding the ion sound speed ($u_{ez}/C_S\sim5$). This could lead to the development of e.g. ion-acoustic or lower hybrid drift instabilities [32], but additional experiments will be needed to investigate this further.

In summary, these experiments have provided a detailed characterization of the interaction layer formed by the collision of two counter-streaming, magnetized, supersonic plasma flows with oppositely oriented magnetic fields. We find that the pile-up, and the subsequent dissipation of magnetic flux, occurs in a narrow region at the boundaries of the interaction layer, forming a bifurcated current structure. The layer has a half-thickness of $\delta\sim c/\omega_{pi}$, and is supported in a quasi-steady state by the balance between the ram pressure of the incoming flow and the thermal

pressure in the layer. Thomson scattering measurements of the plasma parameters show that the plasma inside the layer moves outwards, along the B-field of the incoming plasma flows, with a speed comparable to the inflow velocity. The measured ion temperature is unexpectedly high in comparison with the electron temperature, a situation incompatible with purely resistive heating. It is possible that the observed strong ion heating is driven by the development of kinetic instabilities in the current sheet, but the exact mechanism responsible for this is unknown at present.

This work was supported in part by EPSRC Grant No. EP/G001324/1, and by DOE cooperative agreements No. DE-F03-02NA00057 and No. DE-SC-0001063.

[1] P. Hartigan, A. Frank, J. M. Foster, B. H. Wilde, M. Douglas, P. A. Rosen, R. F. Coker, B. E. Blue, and J. F. Hansen, Astrophys. J. **736**, 29 (2011).

[2] M. Opher, J. F. Drake, M. Swisdak, K. M. Schoeffler, J. D. Richardson, R. B. Decker, and G. Toth, Astrophys. J. **734**, 71 (2011).

[3] J. Pétri and Y. Lyubarsky, Astron. Astrophys. **473**, 683 (2007).

[4] J. Lindl, Phys. Plasmas **2**, 3933 (1995).

[5] D. Biskamp, Phys. Fluids **29**, 1520 (1986).

[6] W. Fox, A. Bhattacharjee, and K. Germaschewski, Phys. Rev. Lett. **106**, 215003 (2011).

[7] G. Fiksel, W. Fox, A. Bhattacharjee, D. H. Barnak, P.-Y. Chang, K. Germaschewski, S. X. Hu, and P. M. Nilson, Phys. Rev. Lett. **113**, 105003 (2014).

[8] M. J. Rosenberg, C. K. Li, W. Fox, I. Igumenshchev, F. H. Séguin, R. P. J. Town, J. A. Frenje, C. Stoeckl, V. Glebov, and R. D. Petrasso, Nat. Commun. **6**, 6190 (2015).

[9] M. J. Rosenberg, C. K. Li, W. Fox, A. B. Zylstra, C. Stoeckl, F. H. Séguin, J. A. Frenje, and R. D. Petrasso, Phys. Rev. Lett. **114**, 205004 (2015).

[10] P. M. Nilson, L. Willingale, M. C. Kaluza, C. Kamperidis, S. Minardi, M. S. Wei, P. Fernandes, M. Notley, S. Bandyopadhyay, M. Sherlock, R. J. Kingham, M. Tatarakis, Z. Najmudin, W. Rozmus, R. G. Evans, M. G. Haines, A. E. Dangor, and K. Krushelnick, Phys. Rev. Lett. **97**, 255001 (2006).

[11] H.-S. Park, C. M. Huntington, F. Fiuza, R. P. Drake, D. H. Froula, G. Gregori, M. Koenig, N. L. Kugland, C. C. Kuranz, D. Q. Lamb, M. C. Levy, C. K. Li, J. Meinecke, T. Morita, R. D. Petrasso, B. B. Pollock, B. A. Remington, H. G. Rinderknecht, M. Rosenberg, J. S. Ross, D. D. Ryutov, Y. Sakawa, A. Spitkovsky, H. Takabe, D. P. Turnbull, P. Tzeferacos, S. V. Weber, and A. B. Zylstra, Phys. Plasmas **22**, 056311 (2015).

[12] N. L. Kugland, D. D. Ryutov, P.-Y. Chang, R. P. Drake, G. Fiksel, D. H. Froula, S. H. Glenzer, G. Gregori, M. Grosskopf, M. Koenig, Y. Kuramitsu, C. Kuranz, M. C. Levy, E. Liang, J. Meinecke, F. Miniati, T. Morita, A. Pelka, C. Plechaty, R. Presura, A. Ravasio, B. A. Remington, B. Reville, J. S. Ross, Y. Sakawa, A. Spitkovsky, H. Takabe, and H.-S. Park, Nat. Phys. **8**, 809 (2012).

[13] K. M. Schoeffler, N. F. Loureiro, R. A. Fonseca, and L. O. Silva, Phys. Rev. Lett. **112**, 175001 (2014).

[14] I. H. Mitchell, J. M. Bayley, J. P. Chittenden, J. F. Worley, A. E. Dangor, M. G. Haines, and P. Choi, Rev. Sci. Instrum. **67**, 1533 (1996).

[15] A. J. Harvey-Thompson, S. V. Lebedev, S. N. Bland, J. P. Chittenden, G. N. Hall, A. Marocchino, F. Suzuki-Vidal, S. C. Bott, J. B. A. Palmer, and C. Ning, Phys. Plasmas **16**, 022701 (2009).

[16] S. V. Lebedev, F. N. Beg, S. N. Bland, J. P. Chittenden, A. E. Dangor, M. G. Haines, K. H. Kwek, S. A. Pikuz, and T. A. Shelkovenko, Phys. Plasmas **8**, 3734 (2001).

[17] J. Greenly, M. Martin, I. Blesener, D. Chalenski, P. Knapp, R. McBride, B. R. Kusse, and D. a. Hammer, in *AIP Conf. Proc.* (AIP, 2009), pp. 53–56.

[18] V. V. Aleksandrov, V. A. Barsuk, E. V. Grabovski, A. N. Gritsuk, G. G. Zukakishvili, S. F. Medovshchikov, K. N. Mitrofanov, G. M. Oleinik, and P. V. Sasorov, Plasma Phys. Reports **35**, 200 (2009).

[19] S. V. Lebedev, L. Suttle, G. F. Swadling, M. Bennett, S. N. Bland, G. C. Burdiak, D. Burgess, J. P. Chittenden, A. Ciardi, A. Clemens, P. de Grouchy, G. N. Hall, J. D. Hare, N. Kalmoni, N. Niasse, S. Patankar, L. Sheng, R. A. Smith, F. Suzuki-Vidal, J. Yuan, A. Frank, E. G. Blackman, and R. P. Drake, Phys. Plasmas **21**, 056305 (2014).

[20] G. F. Swadling, S. V. Lebedev, G. N. Hall, S. Patankar, N. H. Stewart, R. A. Smith, A. J. Harvey-Thompson, G. C. Burdiak, P. de Grouchy, J. Skidmore, L. Suttle, F. Suzuki-Vidal, S. N. Bland, K. H. Kwek, L. Pickworth, M. Bennett, J. D. Hare, W. Rozmus, and J. Yuan, Rev. Sci. Instrum. **85**, 11E502 (2014).

[21] G. F. Swadling, S. V. Lebedev, A. J. Harvey-Thompson, W. Rozmus, G. C. Burdiak, L. Suttle, S. Patankar, R. A. Smith, M. Bennett, G. N. Hall, F. Suzuki-Vidal, and J. Yuan, Phys. Rev. Lett. **113**, 1 (2014).

[22] G. F. Swadling, S. V. Lebedev, N. Niasse, J. P. Chittenden, G. N. Hall, F. Suzuki-Vidal, G. Burdiak, A. J. Harvey-Thompson, S. N. Bland, P. De Grouchy, E. Khoory, L. Pickworth, J. Skidmore, and L. Suttle, Phys. Plasmas **20**, 022705 (2013).

[23] D. H. Froula, S. H. Glenzer, N. C. J. Luhmann, and J. Sheffield, *Plasma Scattering of Electromagnetic Radiation*, 2nd Ed. (Elsevier, 2011).

[24] G. Espinosa, J. M. Gil, R. Rodriguez, J. G. Rubiano, M. A. Mendoza, P. Martel, E. Minguez, F. Suzuki-Vidal, S. V. Lebedev, G. F. Swadling, G. Burdiak, L. A. Pickworth, and J. Skidmore, High Energy Density Phys. **17**, 74 (2015).

[25] F. Suzuki-Vidal, S. V. Lebedev, A. Ciardi, L. A. Pickworth, R. Rodriguez, J. M. Gil, G. Espinosa, P. Hartigan, G. F. Swadling, J. Skidmore, G. N. Hall, M. Bennett, S. N. Bland, G. Burdiak, P. de Grouchy, J. Music, L. Suttle, E. Hansen, and A. Frank, Astrophys. J. **815**, 96 (2015).

[26] I. Hutchinson, *Principles of Plasma Diagnostics*, 2nd Ed. (Cambridge University Press, 2005).

[27] R. Drake, *High-Energy-Density Physics* (Springer Berlin Heidelberg, 2006).

[28] G. Fiksel, A. F. Almagri, B. E. Chapman, V. V. Mirnov, Y. Ren, J. S. Sarff, and P. W. Terry, Phys. Rev. Lett. **103**, 1 (2009).
[29] Y. Ono, M. Yamada, and T. Akao, Phys. Rev. Lett. **76**, 3328 (1996).
[30] M. Yamada, R. Kulsrud, and H. Ji, Rev. Mod. Phys. **82**, 603 (2010).
[31] S. C. Hsu, T. A. Carter, G. Fiksel, H. Ji, R. M. Kulsrud, and M. Yamada, Phys. Plasmas **8**, 1916 (2001).
[32] D. Biskamp, *Magnetic Reconnection in Plasmas* (Cambridge University Press, Cambridge, 2000).